First Frequency-Domain Interferometry Observations of Large-Scale Vertical Motion in the Atmosphere

ANDREAS MUSCHINSKI*

Atmospheric Technology Division, National Center for Atmospheric Research, Boulder, Colorado

PHILLIP B. CHILSON+

Max-Planck Institut für Aeronomie, Katlenburg-Lindau, Germany

STEFAN KERN AND JOST NIELINGER

Institut für Meteorologie und Klimatologie, Universität Hannover, Hannover, Germany

GERHARD SCHMIDT

Max-Planck Institut für Aeronomie, Katlenburg-Lindau, Germany

THOMAS PRENOSIL

Amt für Wehrgeophysik, Traben-Trarbach, Germany

19 March 1997 and 26 August 1998

ABSTRACT

The spatiotemporal distribution of the vertical velocity at synoptic and subsynoptic scales is key to the patterns of weather and climate on earth. On these scales, the vertical velocity is on the order of one to a few centimeters per second, typically about three orders of magnitude smaller than typical horizontal wind velocities. Because of the smallness of large-scale vertical velocities relative to typical horizontal velocities, a direct observation of the large-scale vertical air velocity is extremely difficult.

In a case study on observational material obtained during a 68-h experiment using the SOUSY very high frequency (VHF) radar in the Harz Mountains in Germany, the authors present the first intercomparison between three different sources of physical information that can provide large-scale vertical wind velocities: (i) the Doppler shifts observed with a vertically pointing VHF radar; (ii) the rates of change of the altitudes of refractive-index discontinuities as identified with frequency-domain interferometry (FDI), which is still a relatively unexplored technique in meteorology; and (iii) the output of a regional numerical weather prediction model (NWPM), which has been set up to model the meteorological situation during the observational period.

There are several phenomena that have been known to possibly cause significant biases in mean vertical velocities retrieved from the Doppler shifts measured with vertically pointing clear-air VHF radars: (i) stationary or nonstationary gravity waves with vertical-velocity amplitudes up to the order of 1 m s^{-1}; (ii) stationary or horizontally advected tilted refractive-index discontinuities that are aspect sensitive in the VHF regime; and (iii) a correlation between the radar-reflectivity fluctuations and the vertical-velocity fluctuations within a vertically propagating gravity wave.

On the basis of an intercomparison between the vertical velocities retrieved from (i) ''standard Doppler'' VHF radar observations, (ii) VHF FDI observations, and (iii) the NWPM output, the authors present first evidence that, under ideal conditions, VHF FDI can be used to directly monitor large-scale vertical motion.

1. Introduction

The patterns of weather and climate on earth depend sensitively on the spatial and temporal distributions of the vertical atmospheric motion on regional, synoptic, and global time and length scales (Richardson 1922; Panofsky 1946; Hollmann and Wegner 1959; Kasahara and Washington 1967; White 1983; Van den Dool 1990; Broccoli and Manabe 1992). Modeling with sufficient accuracy the patterns of the large-scale vertical velocity is therefore key to any physical understanding and prog-

* On leave from Institut für Meteorologie und Klimatologie, Universität Hannover, Hannover, Germany.

+ Current affiliation: Swedish Institute of Space Physics, Kiruna, Sweden.

Corresponding author address: Dr. Andreas Muschinski, CIRES, University of Colorado/NOAA, NOAA/Environmental Technology Laboratory, 325 Broadway, R/E/ET4, Boulder, CO 80303.
E-mail: amuschinski@etl.noaa.gov

nosis of the appearance and disappearance of large-scale precipitation and cloudiness, and it is a prerequisite of numerical weather forecasting and climate modeling. Vertical air velocities at horizontal length scales of the order of and larger than 100 km amount typically to not more than one or a few centimeters per second (Panofsky 1946; Bluestein 1992, 300), about three orders of magnitude smaller than typical horizontal wind velocities. This is why large-scale vertical velocities are on a routine basis not directly measured but indirectly determined from the fields of density and horizontal wind, using the law of the conservation of mass (Richardson 1922). The direct measurement of large-scale vertical velocities is still one of the major challenges in meteorology.

In this note, we present results from the first intercomparison between the following three independent methods to estimate the mean vertical air motion over a given location and during synoptic-scale and subsynoptic-scale time periods. Vertical velocities were taken from observations with a very high frequency (VHF) radar using (i) the ''standard'' Doppler technique and (ii) the frequency domain interferometry (FDI); in addition, vertical velocity estimates from (iii) a regional numerical weather prediction model (NWPM) were considered. Such an intercomparison is essential to establish the accuracy and reliability of vertical velocity data currently available to meteorologists.

2. Clear-air Doppler radar measurements of vertical air motion

a. The standard Doppler technique

VHF radars have proved to be valuable tools to efficiently observe the vertical wind at mesoscales (Klostermeyer 1981; Gage 1990). Although the smallness of synoptic-scale vertical velocities suggests that they are not directly measurable (Bluestein 1992, 313), in recent years it has been demonstrated that such measurements are indeed feasible with VHF radars, at least under suitable meteorological conditions (Nastrom 1984; Nastrom et al. 1985; Balsley et al. 1988; Larsen et al. 1988; Gage et al. 1991) and possibly even with ultra high frequency (UHF) radars (McAfee et al. 1995). Sometimes, however, VHF radar observations of the mean vertical wind are considerably affected by mesoscale phenomena, for example, by tilted quasi-specular layers within a field of gravity waves (Röttger 1981; Gage et al. 1981; Gage 1986), or by more or less quasi-stationary lee waves over mountainous terrain (Ecklund et al. 1982; Ralph et al. 1992; McAfee et al. 1995; Ralph et al. 1997). The so-called downward bias of several centimeters per second, which has been observed in a number of VHF radar measurements of the long-term vertical wind, has been attributed to an intrinsic correlation between radar reflectivity and vertical velocity within a field of upward propagating gravity waves (Nastrom and VanZandt 1994; Nastrom et al. 1998). Recently, it has been pointed out that a nonzero correlation between Doppler velocities and tilting angles of quasi-specular layers in a region of Kelvin–Helmholtz instability can also give rise to a bias, in particular in the lower (downward bias) and upper (upward bias) shear zones of jet streams (Muschinski 1996). The tilting angles can be measured using the spaced antenna technique, and such data have been used to improve the vertical-velocity data (Larsen and Röttger 1991; Palmer et al. 1991; Chau and Balsley 1998).

b. Frequency-domain interferometry

FDI may be seen as the simplest version of a discontinuous frequency chirping technique for pulsed Doppler radars. FDI was proposed by Stitt and Bowhill (1986) and first realized for atmospheric radars by Kudeki and Stitt (1987). Amplitudes and phases of the Doppler signals are measured quasi-simultaneously at two closely spaced carrier frequencies instead of at a single frequency, which is usually done and that we refer to as the standard Doppler technique (cf. e.g., Röttger and Larsen 1990; Doviak and Zrnić 1993). Using a vertically pointing radar, the FDI technique at frequencies in the VHF regime allows altitudes and thicknesses of thin persistent layers of refractive-index irregularities in the clear atmosphere to be measured with a resolution of the order of the radar wavelength. The wavelength is usually at least one order of magnitude smaller than the pulse length, which determines the ''conventional'' range resolution of pulsed Doppler radars, $\Delta r = c\tau/2$, where c is the velocity of light and τ is the pulse duration. In other words, the FDI technique allows a fine localization of scatterers with respect to the radial coordinate to be performed, which is impossible when using only a single carrier frequency. Altitude and thickness of a layer within the illuminated range are calculated from phase and magnitude, respectively, of the complex correlation coefficient of the two Doppler time series measured quasi-simultaneously at the two different carrier frequencies. Although two-frequency FDI enables one to unambiguously identify only one layer per control volume, it works quite well in the free troposphere where the vertical spacing between major discontinuities is often larger than the conventional range resolution.

The FDI technique has been implemented at a number of VHF radars and now may be seen as a standard technique, at least in the VHF regime (Cohn and Chilson 1995; Hocking 1997). FDI is, in contrast to the Doppler technique, a direct method of tracking discontinuities in the vertical profiles of temperature and humidity. Nevertheless—and this is to some extent surprising—there has not been much use made of this technique in the meteorological community. In their pioneering paper, which dealt with FDI observations of layers in the mesosphere above Peru, Kudeki and Stitt (1987) pointed

out that, ''Their [the layers'] vertical motion are generally consistent with vertical Doppler velocity estimates.'' The purpose of our experiment in March 1995 was to measure altitudes and thicknesses of scattering layers in the troposphere and lower stratosphere, and to determine to what extent an agreement between Doppler velocities and ''FDI velocities'' could be verified.

3. Setup of observation and simulation

a. Observation

Vertical wind velocities in the middle troposphere were measured with the SOUSY VHF radar, which is located in the Harz Mountains in northern Germany (Czechowsky et al. 1984). Data were taken during the 68-h period between 1200 UTC 10 March and 0800 UTC 13 March 1995. The radar was upgraded for FDI capability in 1994 (Chilson and Schmidt 1996), and during the March 1995 experiment, it was operated in a two-frequency FDI mode. The two carrier frequencies were 53.25 MHz (wavelength 5.63 m) and 53.75 MHz (wavelength 5.58 m). Overlapping single pulse and coded pulse measurements were made; see Chilson et al. (1997) for details of the radar setup.

The pulse length was 2 μs, corresponding to a conventional altitude resolution of 300 m. For the entirety of the observations, the radar was operated in an FDI mode; it transmitted and received alternatingly at each of the two carrier frequencies. With the exception of 11-min interruptions every 66 min for horizontal wind measurements, the radar beam was pointed vertically. Every 13 s, two 64-element complex time series were obtained for each range gate and for each frequency, providing an estimate of layer altitude, layer thickness, and two values for echo intensity, Doppler velocity, and spectral width, respectively. Because of the good time resolution, we were able to study in detail Kelvin–Helmholtz billows at a height of 9 km as a jet stream passed over the radar site during the night from 12 March to 13 March (Chilson et al. 1997). For the first time, it has been possible to resolve with a pulsed clear-air radar upper-tropospheric Kelvin–Helmholtz billows having crest-to-trough amplitudes of less than the radar's conventional range resolution. While in that study we concentrated on layer altitude changes on timescales of the order of 1 min, here we will be considering those at timescales of the order of 1 day.

b. Simulation

A regional NWPM was set up to re-model the meteorological fields during the observation period. We used the Boundary Layer Model (BLM) of the Geophysikalischer Beratungsdienst der Bundeswehr in Traben-Trarbach, Germany (Volkert et al. 1992; Prenosil et al. 1995). The BLM has been providing 36-h weather forecasts twice a day since 1984.

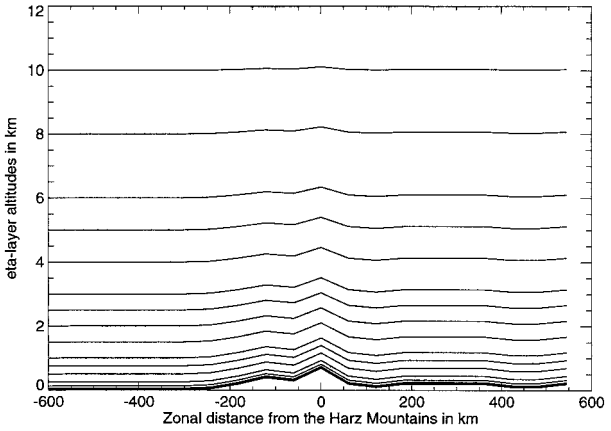

FIG. 1. Zonal vertical cross section of the 17 terrain-following ''η levels'' used in the NWPM, at the latitude of the grid point nearest to the radar site. See caption of Fig. 6 for details.

The model is based on the primitive equations as described by Kasahara and Washington (1967). The grid is horizontally staggered according to Arakawa B (Arakawa and Lamb 1977). In the vertical direction, a terrain-following η coordinate is used with a fixed model top at 12 km above mean sea level (MSL). Figure 1 shows a zonal cut through the model domain at the latitude of the grid point nearest to the radar site. There are 17 levels for pressure and vertical velocity, and there are 16 intermediate levels for zonal wind, meridional wind, temperature, and specific humidity.

The BLM is driven and updated by larger-scale data from the nine-level hemispheric model of the German Weather Service. The horizontal mesh width of the BLM's numerical grid is 63.5 km, and its vertical mesh width increases from 50 m near the surface to 2 km in the tropopause region. The integration in time is carried out in 5-min steps. The vertical velocities are computed diagnostically by using the Richardson equation [Eq. (2.16) in Kasahara and Washington 1967].

4. Data analysis and results

a. Long-lived layers observed with FDI

Figure 2 shows a height–time section of scatterers, for which the altitudes have been determined with the FDI technique. Every 13 s, one scatterer per 300-m height interval has been identified, and each one is represented by a dot in Fig. 2. In Fig. 2 and in the following figures that have the time axis as the abscissa, the time is counted with respect to 0000 UTC 10 March. In Fig. 2, there are regions in the height–time section where the distribution of the retrieved scatterers is fairly homogeneous with respect to height, for example, between 47 and 60 h at around 6-km altitude; in other regions, however, the distribution is very inhomogeneous as a function of altitude, in particular in the lower-left corner

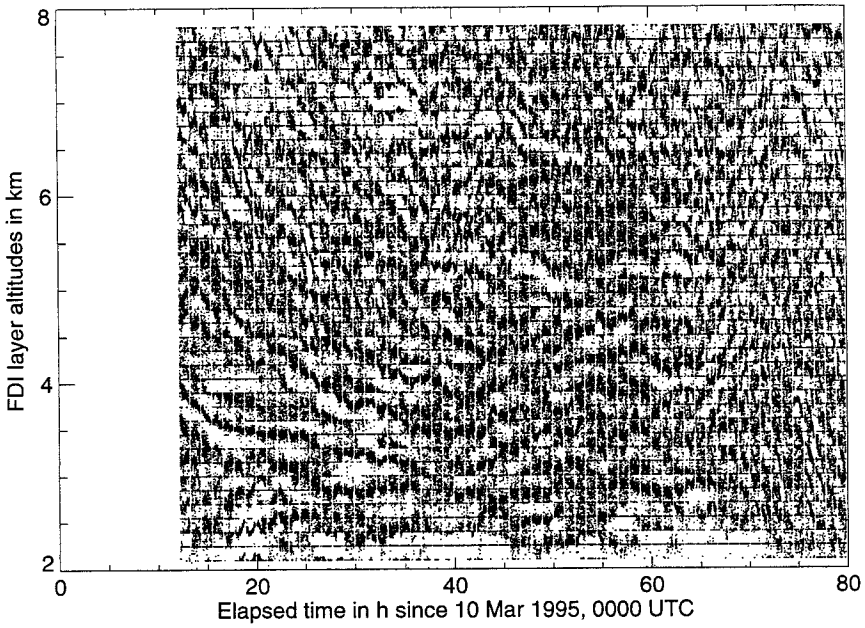

FIG. 2. Height–time sections of scatterers observed with the SOUSY VHF radar operated in an FDI mode.

of the height–time section. Obviously, there are several scatterers that are well defined with respect to the height and continuous with time. In the following, we refer to those features as ''scattering layers'' or simply ''layers.'' The altitude of the layer that starts at 4 km at 12 h decreases with time, and that layer is observed until 27 h, maybe even until 37 h, depending on whether or not one considers the discontinuity at 27 h as the end of the first layer and the beginning of a second layer. Although not as clearly displayed as the layer just mentioned, Fig. 2 exhibits quite a number of long-lived layers during the first two-thirds of the observation period. At altitudes above 3 km and during the first third of the observation period, their altitudes in general decrease at a rate of 750 m during 10 h, that is, at about 2 cm s^{-1}. Below about 3 km, the layer altitudes do not change as systematically as in the upper levels. Sometimes the layer altitudes exhibit oscillations. For example, around 20 h the layer at 2.4 km oscillates with an amplitude of about 150 m and a period of about 1 h.

During the middle third of the observation period, that is, between, say, 40 and 60 h at altitudes between about 3 and 6 km, there appears to be a reversal from an apparent downward motion to an apparent upward motion. After about 60 h, it is hard to recognize any continuity with time, but if one looks more closely one clearly identifies upward and downward moving layers with an apparent vertical velocity that is significantly larger than the 2 cm s^{-1} mentioned above. In the lower-right corner of Fig. 2, a typical apparent downward velocity is 10 cm s^{-1}.

b. Doppler velocities and vertical velocities obtained with the NWP model

Figures 3 and 4 show time series of vertical velocities as obtained from the NWPM and from the VHF radar Doppler shifts in the lower troposphere, that is, at 2.5, 3.0, and 3.5 km (Figs. 3a, 3b, and 3c, respectively), and in the upper troposphere, that is, at 7.0, 8.0, and 9.0 km (Figs. 4a, 4b, and 4c, respectively).

The solid lines with no symbols represent the vertical velocities as obtained from the NPWM. The dotted lines are the rates of change, $\partial z_\Theta/\partial t$, of the altitudes of the surfaces of the potential temperature as obtained from the NWPM data at the level under consideration above the grid point nearest to the experimental site:

$$\frac{\partial z_\Theta}{\partial t} = w - \left(u\frac{\partial \Theta}{\partial x} + v\frac{\partial \Theta}{\partial y}\right)\left(\frac{\partial \Theta}{\partial z}\right)^{-1}. \qquad (1)$$

Here, u and v are the zonal and meridional components of the wind vector, respectively; Θ is the potential temperature; and x, y, and z are the zonal, meridional, and vertical coordinates of the meteorological coordinate system, respectively. In other words, $\partial z_\Theta/\partial t$ represents the local apparent vertical velocity of potential temperature surfaces, where the contribution due to the horizontal advection of tilted surfaces has been taken into account. In the following, we refer to $\partial z_\Theta/\partial t$ obtained from the NWPM as the ''simulated apparent vertical velocity.'' The solid lines with triangles represent 3-h averages of the vertical velocities retrieved directly from

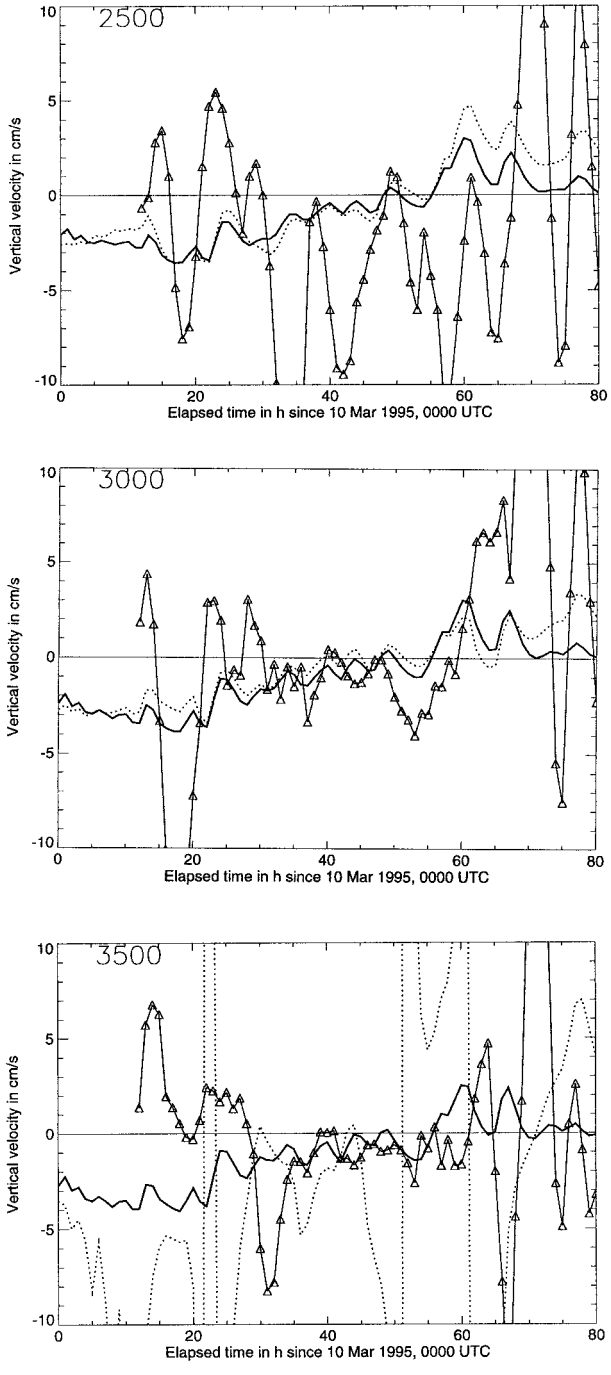

FIG. 3. Time series of vertical velocities in the lower troposphere at (a) 2.5 km MSL, (b) 3.0 km MSL, and (c) 3.5 km MSL. Solid lines with no symbols are the STW, dotted lines are the SAW, and the solid lines with triangles are 3-h averages of the DW. (The acronyms are defined in Table 1.)

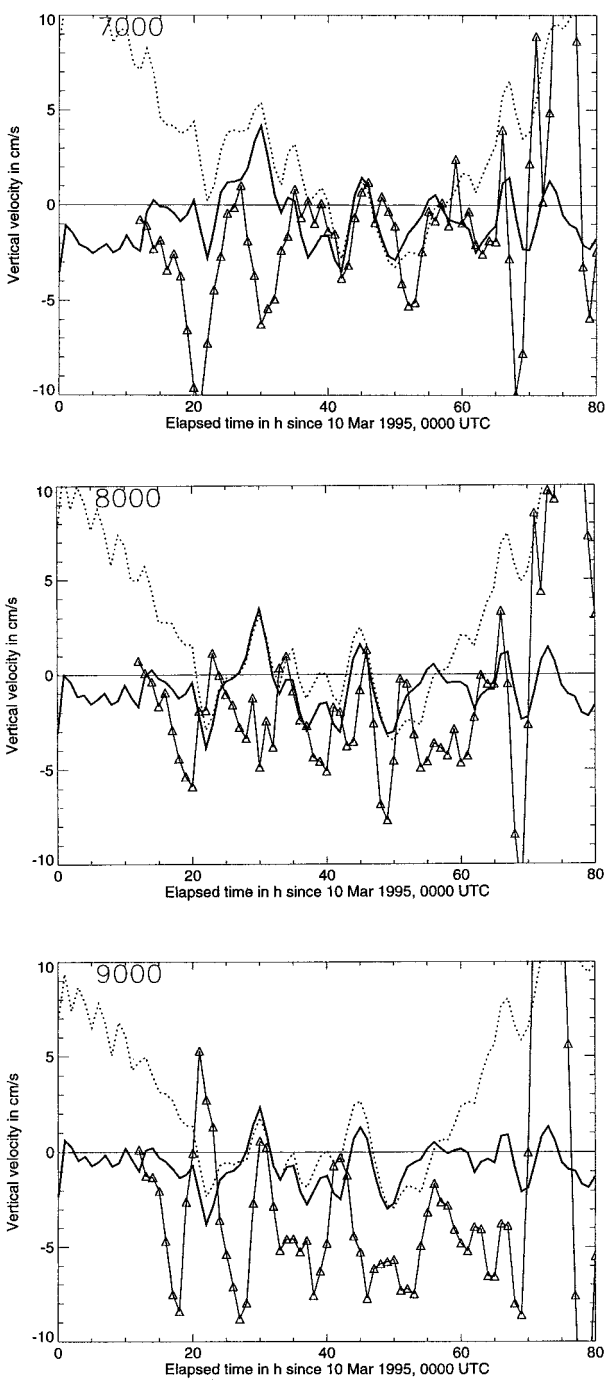

FIG. 4. Same as Fig. 3 but for the upper troposphere: (a) 7.0 km MSL, (b) 8.0 km MSL, and (c) 9.0 km MSL.

the Doppler shifts measured with the vertically pointing SOUSY VHF radar.

Figure 5 shows a sequence of four vertical profiles of 12-hourly averages of vertical velocities. The solid lines with the squares are vertical velocities obtained from the NWPM. The solid lines with the small diamonds are Doppler-velocity profiles obtained from single-pulse data, and those with the small triangles are Doppler-velocity profiles obtained from coded-pulse data. In most cases, the difference between the two Doppler-velocity values is smaller than 1 cm s^{-1}, providing confidence that the variability of the Doppler

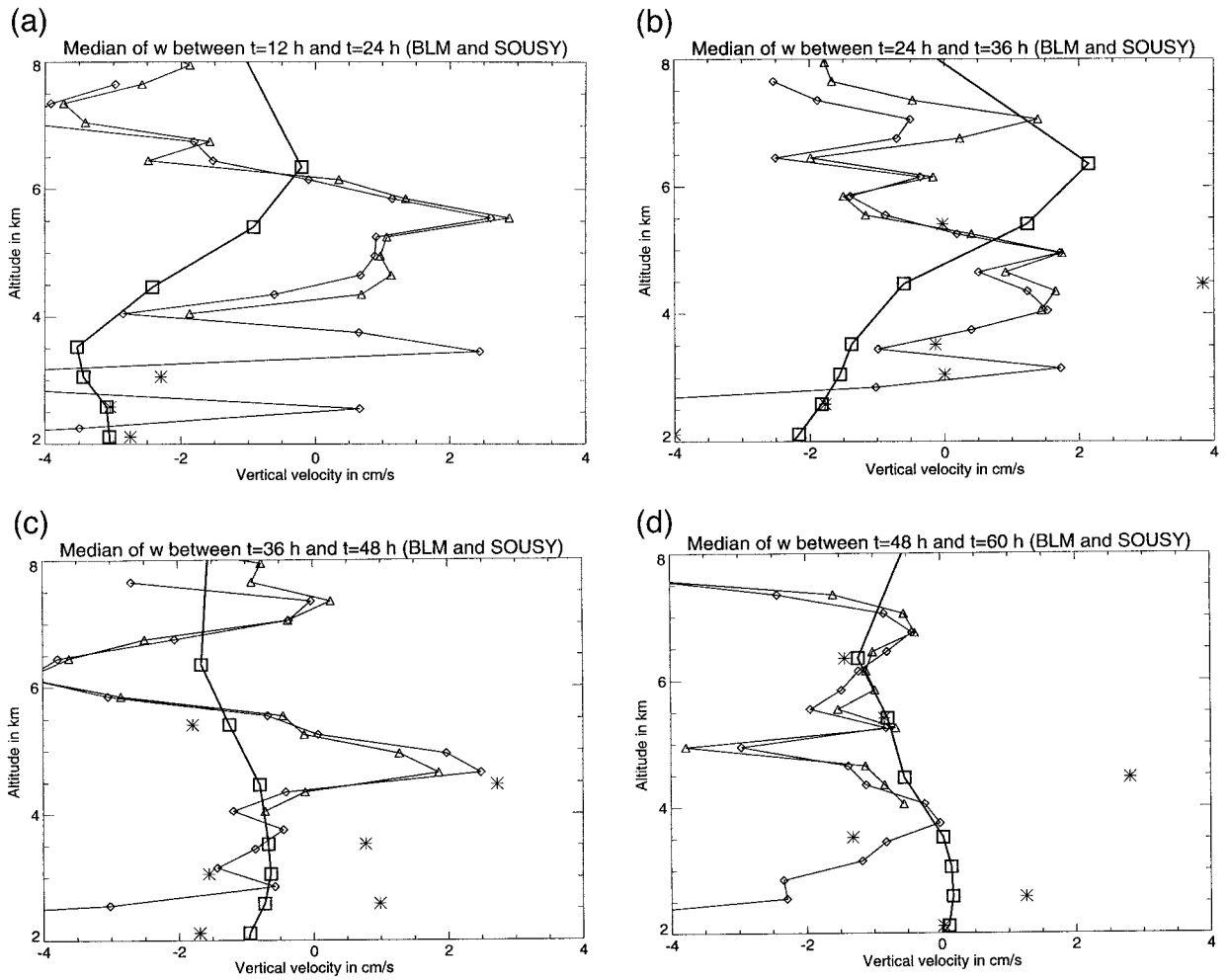

FIG. 5. Vertical profiles of 12-h averages of vertical-velocity estimates: (a) between 12 and 24 h, (b) between 24 and 36 h, (c) between 36 and 48 h, and (d) between 48 and 60 h. Solid lines with squares are STW; solid lines with diamonds (triangles) are DW retrieved from single-pulse (pulse coded) radar data; asterisks are SAW. Abbreviations are explained in section 5a.

velocities with respect to time and height as shown in Fig. 5 is to be interpreted physically and is not to be attributed to noisy radar data or to artifacts caused by the pulse-coding procedure. The asterisks are the 12-hourly averages of the apparent vertical velocities obtained from the NWPM, as defined above.

Figure 6 shows three height–time sections of ''virtual layers,'' that is, the altitudes of idealized horizontal isosurfaces that are vertically advected according to the time-dependent vertical-velocity profile $w(z, t)$ as provided by the NWPM for a specific grid point. Those altitudes have been calculated as follows:

$$z_i(t) = z_i(t_0) + \int_0^t w(z(t'), t')\, dt'. \qquad (2)$$

Here, $z_i(t_0)$ have been arbitrarily chosen equal to the altitudes of the levels of the numerical grid of the NWPM (see Fig. 1) at three specific grid points, where t_0 is 12 h, that is, the time of the beginning of the observation period. Figure 6b has been obtained from the NWPM data at the grid point nearest to the radar site, Fig. 6a for the adjacent grid point 63.5 km to the west, and Fig. 6c for the adjacent grid point 63.5 km to the east. Obviously, the layer altitude patterns shown in the three panels of Fig. 6 differ significantly from each other. While all three panels show a downward motion of about 4 cm s^{-1} between 12 and 25 h in the lower troposphere, that is, below 4 km, there is almost no agreement at later times or at higher altitudes. Figure 6 will also be referred to in section 5e, where we will discuss the horizontal homogeneity of the vertical-velocity field.

c. Height–time sections of wind speed and the potential temperature

Figure 7 shows a height–time section of the horizontal wind velocity obtained from the NWPM. At altitudes

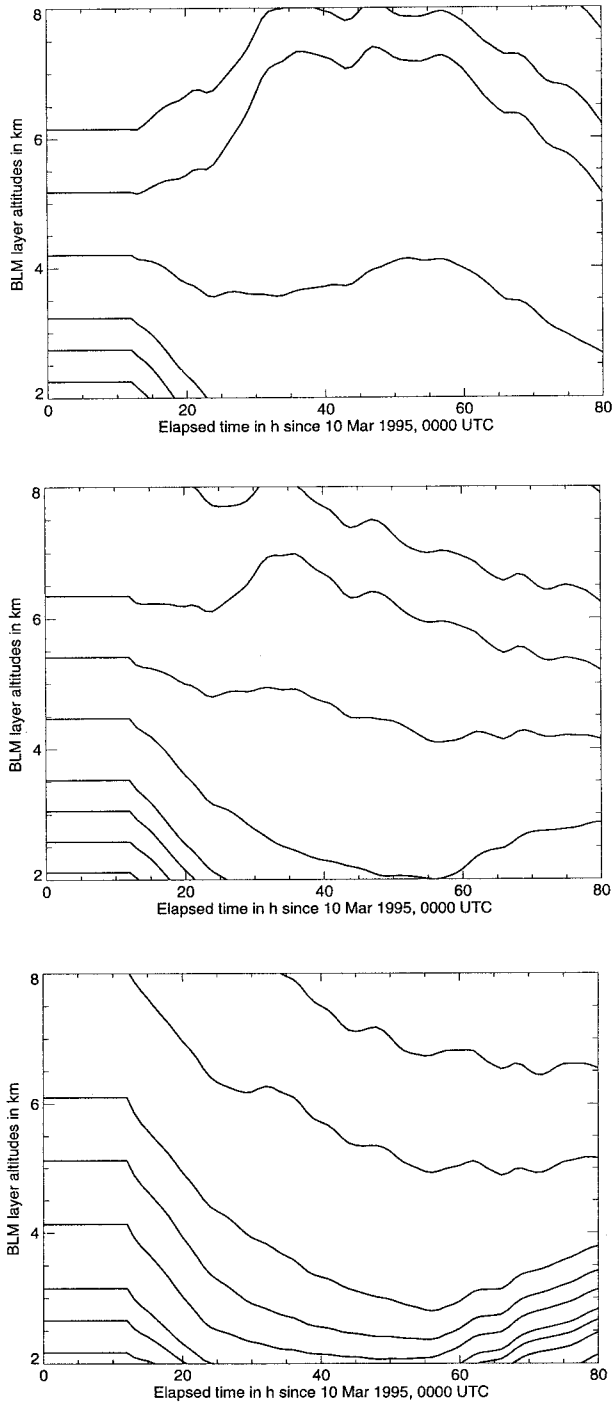

FIG. 6. Height–time sections of isosurfaces of a passive scalar, computed (assuming horizontal homogeneity) from the height–time sections of the NWPM-predicted true vertical wind velocity at three zonally adjacent grid points of the NWPM close to the site of the SOUSY VHF radar (51.70°N, 10.50°E): (a) 51.71°N, 10.00°E, near Northeim at the western rim of the Harz Mountains; (b) 51.70°N, 10.88°E, about 30 km east of the radar site; (c) 51.69°N, 11.76°E, about 90 km east of the radar site.

between 2 and 4 km MSL, the horizontal wind is mostly smaller than 5 m s^{-1} between 0 and 60 h, and it increases to somewhat beyond 10 m s^{-1} at later times. In the upper troposphere, the modeled horizontal wind is up to about 30 m s^{-1} at the beginning and at the end of the observation period but it decreases to about 10 m s^{-1} during the middle third of the observation period. Figure 8 shows a height–time section of the potential temperature obtained from the NWPM. Both height–time sections are for the grid point nearest to the radar site.

5. Discussion

a. Definition, observation, and simulation of vertical velocity

Before we discuss in some more detail the advantages and disadvantages of the different techniques to retrieve vertical velocities from observed or simulated data, we have to define what we mean by ''vertical velocity.''

From the conceptual point of view, we have to distinguish between the ''true'' and the ''apparent'' vertical velocity. The true vertical wind velocity (TW) is by definition the vertical component of the three-dimensional wind velocity vector. As the apparent vertical velocity (AW), however, we define the rate of change of the altitudes of quasi-horizontal surfaces of a specific atmospheric scalar at the altitude under consideration. Note that different scalars have a priori different apparent vertical velocities. Correspondingly, from the simulation point of view we have to distinguish between the simulated true vertical velocity (STW) and the simulated apparent vertical velocity (SAW). If there is no horizontal wind or if there is no tilting of the isosurfaces, that is, if the distribution of the specific scalar is horizontally homogeneous, TW and AW are equal to each other.

With respect to the observational material presented here, we have to distinguish between the ''Doppler velocity'' (DW) and the ''FDI velocity'' (FDIW). The DW is obtained from the Doppler shift observed with a vertically pointing Doppler radar. The FDIW is the rate of change of the altitude of a scattering layer identified and tracked at a certain height. The vertical velocities introduced in this section are listed in Table 1.

b. Advection of tilted layers

Figure 2 shows long-lived scattering layers in the troposphere. If a layer is visible for 1 day (about 10^5 s) above the radar site and if the horizontal wind speed is 10 m s^{-1}, the layer's horizontal extent in the streamwise direction is of the order of 1000 km. Here we assume that the layers are not locally generated.

If such a layer is tilted about a small angle $\Delta\alpha$ with respect to the horizontal plane in the streamwise direction, the contribution of the horizontal advection of tilted layers to the AW amounts to $v\,\Delta\alpha$, where v is the

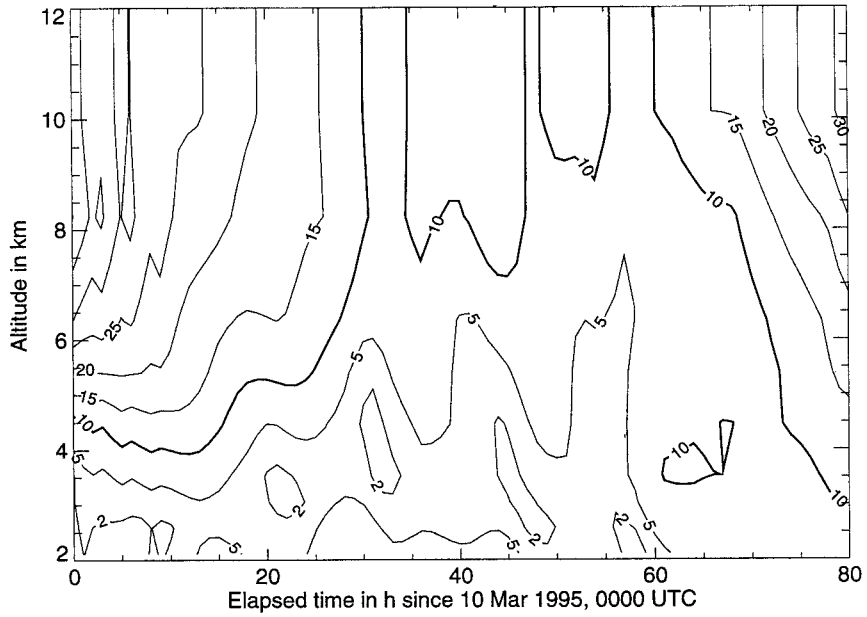

FIG. 7. Height–time section of the horizontal wind speed at the grid point nearest to the radar site, remodeled with the NWPM. Wind speeds are given in m s^{-1}.

horizontal wind speed. We conclude that $v\,\Delta\alpha$ must not exceed 1 cm s^{-1} if the contribution of the horizontal advection of tilted layers to the AW is required to be smaller than 1 cm s^{-1}, corresponding to a $\Delta\alpha$ smaller than 10^{-3} in the case of $v = 10$ m s^{-1}, and smaller than 2×10^{-4} in the case of $v = 50$ m s^{-1}. We conclude that even at moderate horizontal wind speeds, small tilting angles can cause apparent vertical velocities that exceed typical synoptic-scale true vertical velocities.

Figures 3a and 3b show that the difference between STW and SAW is about 1 cm s^{-1} at 2.5- and 3.0-km altitudes, in agreement with the small horizontal wind velocities in that altitude range. The erratic behavior of the SAW at 3.5 km (Fig. 3c) is to be attributed to the

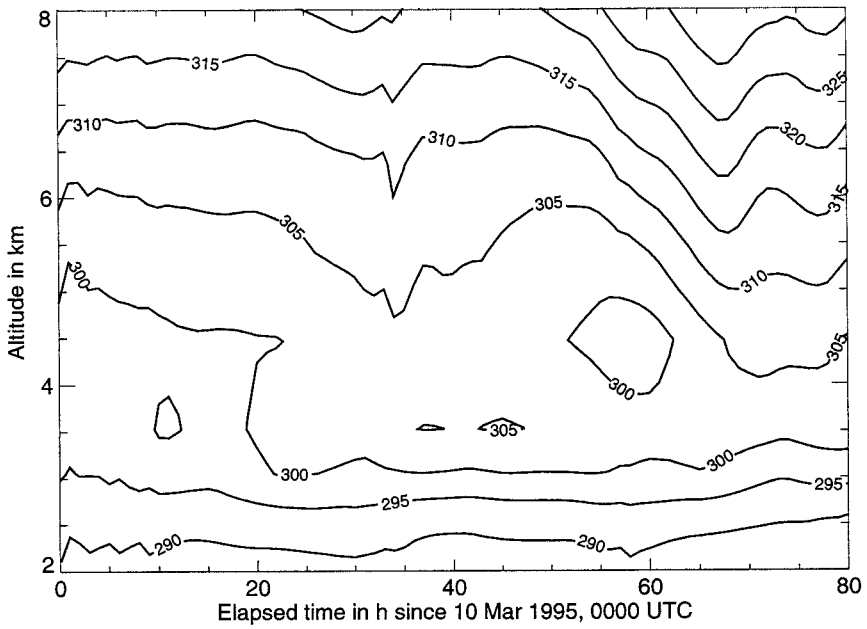

FIG. 8. Height–time section of the potential temperature at the grid point nearest to the radar site, remodeled with the NWPM. Potential temperatures are given in K.

TABLE 1. Definitions of vertical velocity acronyms.

Acronym	Definition
TW	True vertical velocity
AW	Apparent vertical velocity
STW	Simulated true vertical velocity
SAW	Simulated apparent vertical velocity
DW	Doppler velocity (i.e., the vertical velocity calculated from the first moment of the Doppler shift measured with a vertically pointing VHF radar)
FDIW	FDI velocity (i.e., the vertical velocity estimated from the rate of change of the altitude of a scattering layer)

nearly adiabatic stratification at that altitude (see Fig. 8), causing an unrealistically large scatter of the numerical values of the second term on the rhs of Eq. (1). Figures 4a, 4b, and 4c show that at the beginning and at the end of the observation period when the horizontal wind speed was high, STW and SAW differ from each other by about 10 cm s^{-1} in the upper troposphere, and during the middle third of the period, which was characterized by smaller horizontal wind velocities, the difference between STW and SAW amounts to about 1 or 2 cm s^{-1}.

c. The physical nature of the scattering layers

For several decades, there has been a controversy over whether the layers seen by UHF–VHF clear-air radars are turbulent layers or laminar discontinuities (e.g., Gage 1990, 542ff.). Recent in situ observations of the submeter-scale microstructure of temperature and humidity in the lower free troposphere (Muschinski and Wode 1997, 1998) have provided direct evidence for the existence of submeter-scale temperature and humidity discontinuities as well as for the existence of thin turbulent layers. Although it appears plausible that laminar discontinuities dominate at large Richardson numbers and turbulent layers at smaller Richardson numbers, we are not able to answer the question of whether the structures shown in Fig. 2 are laminar refractive-index discontinuities or thin turbulent layers.

d. Quasi-stationary mountain waves

The area observed with a vertically or nearly vertically pointing tropospheric clear-air Doppler radar is typically between 100 m and 1 km in diameter. The grid spacing of the NWPM used in our study, however, is 63.5 km. Therefore, the radar observed vertical velocities at horizontal length scales that were about two orders of magnitude smaller than the smallest resolvable horizontal length scales in the NWPM.

Mountain waves are phenomena that have typical length scales larger than the radar's observation volume but smaller than the resolution of the NWPM that we used. Since the experiment was carried out in hilly terrain, it is to be expected that the variability of the DW is larger than that of the STW obtained with the NWPM, in agreement with Figs. 3 and 4. Mountain waves have comparatively small length scales but they can persist over many hours. So their possible effects on radar observations on the mean vertical wind have to be taken into account.

Ralph et al. (1997) found that 10% per hour is a typical rate of change of the horizontal wavelength of a nonstationary trapped lee wave. Changes of the wavelength cause changes of the phase of the mountain wave above a fixed location, eventually causing variations of the TW at timescales of the order of 10 h, depending on the details of the flow. The 3-h averages of the Doppler velocities shown in Figs. 3 and 4 do show oscillations in the 10-h regime. Their amplitudes are of the order of only 5 cm s^{-1} and appear to be correlated with the horizontal wind speed, as expected (see, e.g., Ecklund et al. 1982).

e. Observation of large-scale vertical motion using a single radar: Standard Doppler technique versus FDI

Both FDI and the standard Doppler observations are sensitive to refractive-index irregularities within the observation volume. When using FDI to track slow but persistent vertical motion, one makes use of the temporal continuity of scattering layers over many hours. The standard Doppler technique, however, provides one vertical velocity estimate every dwell time, in our case every 13 s, and it does not allow one to use that continuity in time. This indicates that one should expect more robust vertical-velocity estimates from FDI than from the standard Doppler technique if a small vertical velocity persists over many hours.

Consider a horizontally extended refractive-index discontinuity disturbed by a stationary mountain wave field. If there is a synoptic-scale vertical motion, the deformed surface is shifted vertically as a whole, and FDI provides directly the large-scale vertical motion. In contrast, the standard Doppler technique yields a local vertical velocity estimate that depends strongly on the local wave-induced tilt of the scattering layer within the observation volume (Gage et al. 1981; Gage 1986). The FDI velocity, however, does not depend on the local tilting angle under such ideal conditions.

Figure 5 shows that between 12 and 24 h, that is, at the beginning of the observation period, the STW amounts to -3 cm s^{-1} at altitudes below about 5 km. Later, the magnitude of the STW becomes smaller. Figure 6 indicates that below 4 or 5 km, the STW is about the same at three grid points in the vicinity of the radar site, while there is considerable horizontal inhomogeneity of the STW at higher levels. So we concentrate on the period between 12 and 24 h and on the altitude range below 4 km. Figure 2 shows a layer that descends from 4 km at 12 h to 3.4 km at 24 h. Its altitude change rate is -3 cm s^{-1} between 12 and 16 h, and its average

altitude change rate between 12 and 24 h is about -1.5 cm s^{-1}. Magnitude, sign, and trend of the layer's altitude change rate are in agreement with the STW and the SAW as shown in Figs. 3 and 5a, and also with the height–time section of the potential temperature as shown in Fig. 8. The difference between STW and SAW is negligible because of the very small horizontal wind velocity in that region of the height–time section. As shown in Fig. 3, however, the DW does not agree with the FDIW, the STW, and the SAW. The oscillations of the DW between 12 and 24 h may have been caused by quasi-stationary mountain waves above the radar site.

During the first half of the observation period, the radar was in a high pressure area; later, the meteorological situation was characterized by a less anticylonic flow at lower altitudes and by a jet stream in the upper levels (see also Chilson et al. 1997). The change from an anticylonic to a less anticyclonic flow is in qualitative agreement with the strong downward motion at the beginning of the observation period and a weakening of the downward motion at later times. More quantitative support is provided by the NWPM output.

6. Conclusions

In principle, both the standard Doppler technique and the FDI technique can provide information about the mean vertical wind velocity with an accuracy sufficient to resolve synoptic-scale vertical motion. Often, however, such observations are contaminated by waves with comparatively small horizontal length scales and amplitudes significantly larger than typical synoptic-scale vertical velocities. Radar observations of the mean vertical wind can also be affected by tilted refractive-index surfaces that are horizontally advected through the observation volume.

In this note, on the basis of material obtained in a case study covering a period of 68 h, we have presented and discussed vertical-velocity estimates from three different sources: (i) the Doppler shifts measured with the standard Doppler technique, (ii) the rates of change of layer altitudes monitored with FDI, and (iii) results from a numerical weather prediction model (NWPM).

It has been shown that under ideal conditions (presence of well-defined and long-lived scattering layers; small horizontal wind speed), the FDI technique can provide large-scale vertical-velocity estimates with an accuracy of about 1 cm s^{-1}. It appears that FDI velocities observed above hilly terrain are not as severely affected by mountain waves as Doppler velocities are, provided the advection of tilted layers can be neglected and the mountain waves are sufficiently stationary. It is obvious, however, that such ideal conditions are the exception rather than the rule. It is to be expected that in most cases horizontal advection of tilted layers dominates the temporal change of scattering layers observed with FDI above the radar. Therefore, there is little hope that FDI can be used to track true large-scale vertical velocities on a routine basis.

A question that is in some sense complementary to the question of how to track true vertical motion, and which we have left unanswered in this study, is, under which circumstances may a height–time section of scattering layers as observed with VHF FDI be interpreted as the height–time section of the potential temperature above the radar site?

Although the material presented in this case study is limited, it is probably not premature to conclude that frequency-domain interferometry is a promising research technique for future synoptic meteorology.

Acknowledgments. Thanks are due to the technical staff of the Max-Planck Institut für Aeronomie (Katlenburg-Lindau, Germany) for operating the SOUSY VHF radar, and to the Amt für Wehrgeophysik (Traben-Trarbach, Germany) for providing the boundary layer model for this study. One of us (AM) appreciates interesting discussions with and helpful comments by D. Carlson, S. Cohn, E. E. Gossard, D. Lenschow, F. M. Ralph, R. G. Strauch, and T. E. VanZandt, as well as the hospitality of NCAR's Atmospheric Technology Division. In particular, we thank the three anonymous reviewers for their valuable comments. AM's research stay at NCAR was funded by the Deutsche Forschungsgemeinschaft.

REFERENCES

Arakawa, A., and V. R. Lamb, 1977: Computational design of the basic dynamical processes of the UCLA general circulation model. *General Circulation Models of the Atmosphere,* J. Chang, Ed., *Methods in Computational Physics,* Vol. 17, Academic Press, 173–265.

Balsley, B. B., W. L. Ecklund, D. A. Carter, A. C. Riddle, and K. S. Gage, 1988: Average vertical motions in the tropical atmosphere observed by a radar wind profiler on Pohnpei (7°N latitude, 157°E longitude). *J. Atmos. Sci.,* **45,** 396–405.

Bluestein, H. B., 1992: *Synoptic-Dynamic Meteorology in Midlatitudes.* Vol. 1. Oxford University Press, 431 pp.

Broccoli, A. J., and S. Manabe, 1992: The effects of orography on midlatitude Northern Hemisphere dry climates. *J. Climate,* **5,** 1181–1201.

Chau, J. L., and B. B. Balsley, 1998: Interpretation of angle-of-arrival (AOA) measurements in the lower atmosphere using spaced antenna radar systems. *Radio Sci.,* **33,** 517–533.

Chilson, P. B., and G. Schmidt, 1996: Implementation of frequency domain interferometry at the SOUSY VHF Radar: First results. *Radio Sci.,* **31,** 263–272.

——, A. Muschinski, and G. Schmidt, 1997: First observations of Kelvin–Helmholtz billows in an upper-level jet stream using VHF frequency domain interferometry. *Radio Sci.,* **32,** 1149–1160.

Cohn, S. A., and P. B. Chilson, 1995: NCAR workshop on multiple-receiver and multiple-frequency techniques for wind profiling. *Bull. Amer. Meteor. Soc.,* **76,** 2474–2480.

Czechowsky, P., G. Schmidt, and R. Rüster, 1984: The mobile SOUSY Doppler radar: technical design and first results. *Radio Sci.,* **19,** 441–450.

Doviak, R. J., and D. S. Zrnić, 1993: *Doppler Radar and Weather Observations.* 2d ed. Academic Press, 562 pp.

Ecklund, W. L., K. S. Gage, B. B. Balsley, R. G. Strauch, and J. L.

Green, 1982: Vertical wind variability observed by VHF radar in the lee of the Colorado Rockies. *Mon. Wea. Rev.*, **110,** 1451–1457.

Gage, K. S., 1986: Implications of tilting of stable layers on atmospheric measurements by clear-air Doppler radars. Preprints, *23d Conf. on Radar Meteorology,* Snowmass, CO, Amer. Meteor. Soc., 30–33.

——, 1990: Radar observations of the free atmosphere: Structure and dynamics. *Radar in Meteorology,* D. Atlas, Ed., Amer. Meteor. Soc., 534–565.

——, D. A. Carter, and W. L. Ecklund, 1981: The effect of gravity waves on specular echoes observed by the Poker Flat MST Radar. *Geophys. Res. Lett.*, **8,** 599–602.

——, J. R. McAfee, D. A. Carter, W. L. Ecklund, A. C. Riddle, G. C. Reid, and B. B. Balsley, 1991: Long-term mean vertical motion over the tropical Pacific: Wind-profiling Doppler radar measurements. *Science*, **254,** 1771–1773.

Hocking, W. K., 1997: Recent advances in radar instrumentation and techniques for studies of the mesosphere, stratosphere, and troposphere. *Radio Sci.,* **32,** 2241–2270.

Hollmann, G., and K. O. Wegner, 1959: Approximative Berechnung der Vertikalbewegung ausgewählter Wetterlagen. *Beitr. Phys. Atmos.,* **31,** 200–216.

Kasahara, A., and W. M. Washington, 1967: NCAR global general circulation model of the atmosphere. *Mon. Wea. Rev.*, **95,** 389–402.

Klostermeyer, J., 1981: MST radars: Advanced tools for gravity wave studies. *Nature*, **292,** 107–108.

Kudeki, E., and G. Stitt, 1987: Frequency domain interferometry: A high resolution radar technique for studies of atmospheric turbulence. *Geophys. Res. Lett.*, **14,** 198–201.

Larsen, M. F., and J. Röttger, 1991: VHF radar measurements of in-beam incidence angles and associated vertical-beam radial velocity corrections. *J. Atmos. Oceanic Technol.,* **8,** 478–490.

——, ——, and T. S. Dennis, 1988: A comparison of operational analysis and VHF wind profiler vertical velocities. *Mon. Wea. Rev.*, **116,** 48–59.

McAfee, J. R., K. S. Gage, and R. G. Strauch, 1995: Vertical velocities at Platteville, Colorado: An intercomparison of simultaneous measurements by the VHF and UHF profilers. *Radio Sci.,* **34,** 1027–1042.

Muschinski, A., 1996: Possible effect of Kelvin–Helmholtz instability on VHF radar observations of the mean vertical wind. *J. Appl. Meteor.,* **35,** 2210–2217.

——, and C. Wode, 1997: In situ observations of the sub-meter-scale microstructure of wind, temperature, and humidity in the free troposphere. Preprints, *12th Symp. on Boundary Layers and Turbulence,* Vancouver, BC, Canada, Amer. Meteor. Soc., 370–371.

——, and ——, 1998: First in situ evidence for coexisting submeter temperature and humidity sheets in the lower free troposphere. *J. Atmos. Sci.*, **55,** 2893–2906.

Nastrom, G. D., 1984: Detection of synoptic-scale vertical velocities using an MST radar. *Geophys. Res. Lett.*, **11,** 57–60.

——, and T. E. VanZandt, 1994: Mean vertical motions seen by radar wind profilers. *J. Appl. Meteor.,* **33,** 984–995.

——, W. L. Ecklund, and K. S. Gage, 1985: Direct measurement of large-scale vertical velocities using clear-air Doppler radars. *Mon. Wea. Rev.*, **113,** 708–718.

——, R. Rüster, and G. Schmidt, 1998: The coupling of vertical velocity and signal power observed with the SOUSY VHF Radar. *J. Appl. Meteor.,* **37,** 114–119.

Palmer, R. D., M. F. Larsen, R. F. Woodman, S. Fukao, M. Yamamoto, T. Tsuda, and S. Kato, 1991: VHF radar interferometry measurements of vertical velocity and the effect of tilted refractivity surfaces on standard Doppler measurements. *Radio Sci.,* **26,** 417–427.

Panofsky, H. A., 1946: Methods of computing vertical motions in the atmosphere. *J. Meteor.*, **3,** 45–49.

Prenosil, T., D. Thiel, and H. Kraus, 1995: Frontogenesis and cross frontal circulation in a strong summertime cold front. *Meteor. Atmos. Phys.,* **56,** 181–196.

Ralph, F. M., M. Crochet, and S. V. Venkateswaran, 1992: A study of mountain lee waves using clear-air radar. *Quart. J. Roy. Meteor. Soc.*, **118,** 597–627.

——, P. J. Neiman, T. L. Keller, D. Levinson, and L. Fedor, 1997: Observations, simulations, and analysis of nonstationary trapped lee waves. *J. Atmos. Sci.,* **54,** 1308–1333.

Richardson, L. F., 1922: *Weather Prediction by Numerical Process.* Cambridge University Press, 236 pp.

Röttger, J., 1981: Wind variability in the stratosphere deduced from spaced antenna VHF radar measurements. Preprints, *20th Conf. on Radar Meteorology,* Boston, MA, Amer. Meteor. Soc., 22–29.

——, and M. F. Larsen, 1990: UHF/VHF radar techniques for atmospheric research and wind profiler applications. *Radar in Meteorology,* D. Atlas, Ed., Amer. Meteor. Soc., 235–281.

Stitt, G. R., and S. A. Bowhill, 1986: Improving range resolution with a frequency hopping technique. *Handbook for MAP,* Vol. 20, SCOSTEP Secretariat, University of Illinois, Urbana–Champaign, Urbana, Illinois, 448–457. [Available from SCOSTEP Secretariat, % NOAA/NGDC, 325 Broadway, Boulder, CO 80303.]

Van den Dool, H. M., 1990: Time-mean precipitation and vertical motion patterns over the United States. *Tellus,* **42A,** 51–64.

Volkert, H., M. Kurz, D. Majewski, T. Prenosil, and T. Tafferner, 1992: The front of 8 October 1987—Prediction of three mesoscale models. *Meteor. Atmos. Phys.,* **48,** 179–191.

White, G. H., 1983: Estimates of the seasonal mean vertical velocity fields of the extratropical Northern Hemisphere. *Mon. Wea. Rev.*, **111,** 1418–1433.